View metadata, citation and similar papers at core.ac.uk

brought to you by CORE

provided by Tsukuba Repository

Energetics and electronic structures of MoS2 nanoribbons

著者（英）	Mina MARUYAMA, Susumu OKADA, Hisaki Sawahata
journal or publication title	Japanese Journal of Applied Physics
volume	58
number	7
page range	075002-1-075002-5
year	2019-06
権利	(C)2019 The Japan Society of Applied Physics This is the Accepted Manuscript version of an article accepted for publication in Japanese Journal of Applied Physics. IOP Publishing Ltd is not responsible for any errors or omissions in this version of the manuscript or any version derived from it.The Version of Record is available online at https://doi.org/10.7567/1347-4065/ab2343.
URL	http://hdl.handle.net/2241/00157833

doi: 10.7567/1347-4065/ab2343

Creative Commons : 表示 - 非営利 - 改変禁止
http://creativecommons.org/licenses/by-nc-nd/3.0/deed.ja

Energetics and electronic structures of MoS_2 nanoribbons

Hisaki Sawahata, Susumu Okada, and Mina Maruyama*

Graduate School of Pure and Applied Sciences, University of Tsukuba, 1-1-1 Tennodai, Tsukuba, Ibaraki 305-8571, Japan

We study the energetics and electronic structures of MoS_2 nanoribbons with clean armchair, chiral, and zigzag edges by conducting the first-principle total energy calculations based on the density functional theory. Our calculations showed that the nanoribbon with zigzag edges is the most stable among the ribbons studied here. The ribbons with armchair or near armchair edges are semiconductors with direct band gap at the Γ point, owing to the large edge relaxation reducing unsaturated nature of edge atoms, while the ribbons with zigzag and near zigzag edges are metals with the finite density of state at the Fermi level. According to the asymmetric atomic arrangement in ribbons with the chiral and zigzag edges, they have polarity normal to the ribbon, which monotonically increase with increasing the edge angle.

1. Introduction

An exfoliation of a single layer of a honeycomb covalent network of C atoms, graphene, from graphite opens a new paradigm of material science and engineering.[1)] A honeycomb network attributed from strong covalent bonds among C atoms endows graphene with remarkable physical properties which make it an emerging material for exploring the low-dimensional sciences and for designing various functional devices.[2,3)] High carrier mobility arising from the linear dispersion bands allows it to be a conducting channel for high-speed switching devices, if graphene can have a finite band gap.[4–9)] Following syntheses of graphene,[10–13)] other two-dimensional materials, which basically possess layered structures of the covalent two-dimensional networks, have been exfoliated from their bulk layered structures and been synthesized chemical vapor deposition techniques.[14–17)] These atom-layer materials have versatile physical properties depending on their covalent network topology and constituent elements. Transition metal dichalcogenides (TMDCs), such as MoS_2, $MoSe_2$, WS_2, WSe_2, and $MoTe_2$, are representative example of such atom-layer materials, which consist of an atomic layer of transition metals forming a triangular lattice sandwiched by atomic layers of chalcogens arranged

*E-mail: mmaruyama@comas.frsc.tsukuba.ac.jp

in prismatic manner, resulting in the hexagonal network of these elements with the thickness of about 3Å. The most of them are known to be semiconductors with the direct band gap at the K point,[18] which strongly depend on the constituent elements, even thought their thin films or bulks are indirect band gap semiconductors.[19] According to their chemically inert surfaces owing to the two-dimensional covalent networks, they could be building blocks of various heterostructures each of which layer is bound via weak van der Waals interaction. In such van der Waals heterostructures, because of the variation of the constituent layers, we can tailor their physical properties by assembling and stacking them in an appropriate manner.[20,21]

In addition to the van der Waals heterostructures, atom-layer materials are also starting materials for the other low-dimensional materials, such as tubes, ribbons, and flakes, by imposing additional boundary conditions. A tubular boundary condition on graphene results in carbon nanotubes which are either metals or semiconductors depending on their diameter and atomic arrangements along their circumferences.[22–24] Graphene nanoribbons are the other possible one-dimensional form of graphene derivatives obtained by imposing an open boundary condition. In the case, they have semiconducting, metallic, and magnetic properties depending on their width and edge shapes.[25–28] Because of the confinement effect of electrons, their total energy is inversely proportional to its size where π electrons are distributed.[29] h-BN, known to be an insulating version of graphene, has similar nanostructures with insulating electronic properties, irrespective of their local and global atomic arrangements.[30–32] As the case of graphene and h-BN, TMDCs also possess tubular, striped, and flake morphologies,[33–35] although they have three-atom thickness. Indeed, such nanostructures have experimentally synthesized exhibiting interesting physical properties, part of which is theoretically elucidated. However, comprehensive studies on TMDC nanoribbons are insufficient to date. In particular, a little is know about the energetics and electronic properties of the ribbons in terms of their edge shape.[36,37] Thus, in this work, we aim to clarify the energetics and electronic properties of MoS_2 nanoribbons with various edge shapes to add the theoretical insight into the energetics of TMDC nanoribbons with respect to the edge shape. Our theoretical calculations show a ribbon with zigzag polar edges is the most stable among ribbons studied here, while the chiral edges are energetically unfavorable compared with armchair and zigzag edges. The ribbons with the edges of an armchair (edge angle $\theta = 0°$) and a chiral (edge angle $\theta = 8°$) are semiconductors with the direct band gap. While the rest of the ribbons have metallic

electronic structures owing to the edge geometrical effect.

2. Methods

All calculations were performed in the framework of the density functional theory (DFT)[38,39] using the Simulation Tool for Atom TEchnology (STATE) package.[40] To calculate the exchange-correlation energy among the interacting electrons, we used the generalized gradient approximation (GGA) with the Perdew-Burke-Ernzerhof functional form.[41,42] Ultrasoft pseudopotentials generated using the Vanderbilt scheme were employed to describe the interaction between electrons and nuclei.[43] The valence wave functions and deficit charge density were expanded in terms of the plane-wave basis set with cutoff energies of 25 and 225 Ry, respectively. Integration over the one-dimensional Brillouin zone was carried out using equidistant k-point sampling in which 4 k-points were taken along ribbon direction, corresponding to 32 k-point sampling for the primitive cell of MoS_2. The atomic structure of MoS_2 nanoribbons were optimized until the force acting on each atoms were less than 5 mRy/Å under fixed lateral lattice parameters which correspond with the length calculated by the experimental lattice parameters of bulk MoS_2 (3.15 Å).[17] Because the nanoribbons with chiral and zigzag edges intrinsically possess polar edges owing to the chemical difference between Mo and S atoms, we adopted the effective screening medium (ESM), which allow us to impose the open boundary condition normal to the ribbons, which exclude unphysical electrostatic interaction with the periodic images in the framework of the DFT with plane-wave basis set.[44]

3. Results and discussions

Figure 1 shows the optimized geometries of MoS_2 nanoribbons with armchair ($\theta = 0°$), chiral (θ = 8, 16, and 23°), and zigzag (θ = 30°) clean edges, of which width are about 16 Å. In addition to the ribbon width, the lengths of the ribbons are almost the same each other with the length of about 25 Å containing 48 Mo atoms and 96 S atoms per unit cell, to make the quantitative discussion on their energetics. For the case of the armchair clean edges, there are substantial structural reconstructions near the edge atomic sites where Mo and S atoms shift inward and outward, respectively, owing to their chemical difference [Fig. 1(a)]. Accordingly, the armchair ribbon has buckled edges as the case of h-BN nanoribbons. For the cases of nanoribbons with chiral edges, because the edges contain both armchair and zigzag portions, they have structural

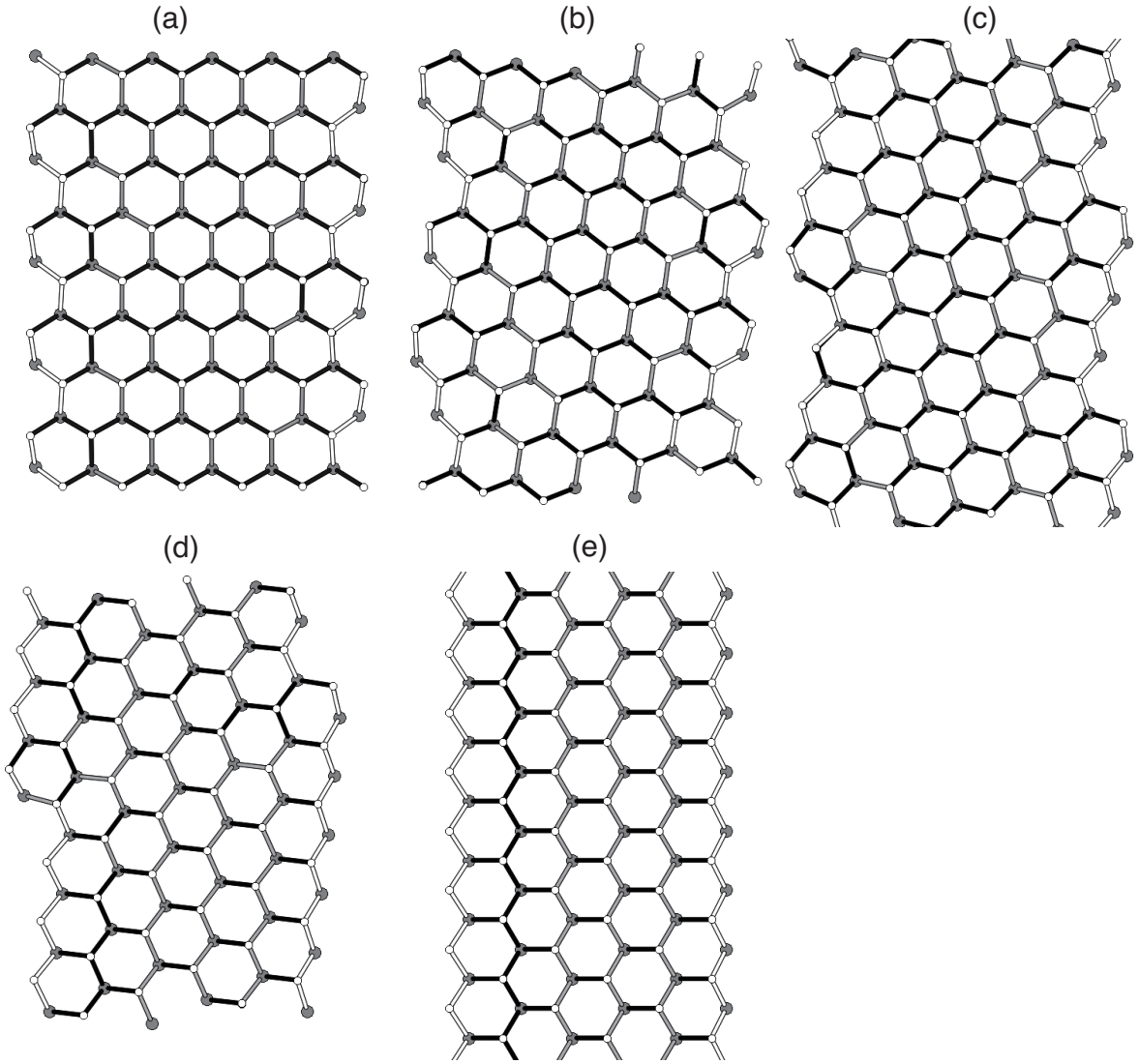

Fig. 1. Optimized geometries of MoS_2 nanoribbons with clean edges of which angles are (a) 0° (armchair), (b) 8°, (c) 16°, (d) 23°, and (e) 30° (zigzag). Black and white circles denote Mo and S atoms, respectively. Dark shaded, pale shaded, and white bonds indicate long (2.41 Å–), equilibrium or bulk (2.41–2.40 Å), and short (–2.40 Å) bonds, respectively.

reconstruction at the edge atomic sites with the armchair shape: Mo and S shift inward and outward, respectively. According to the structural reconstruction, bond lengths are substantially modulated from that of the bulk (equilibrium) value for the ribbons with armchair and chiral edges [Figs. 1(a)-1(d)]. The reconstruction basically decreases the bond length associated with the edge atomic sites, with the increase of the charge density of the edge bond suppressing the unsaturated nature of these atoms. In contrast, the ribbon with zigzag edges seems not to exhibit significant structural reconstructions at their edges, keeping their hexagonal structures not only in inner region but also at

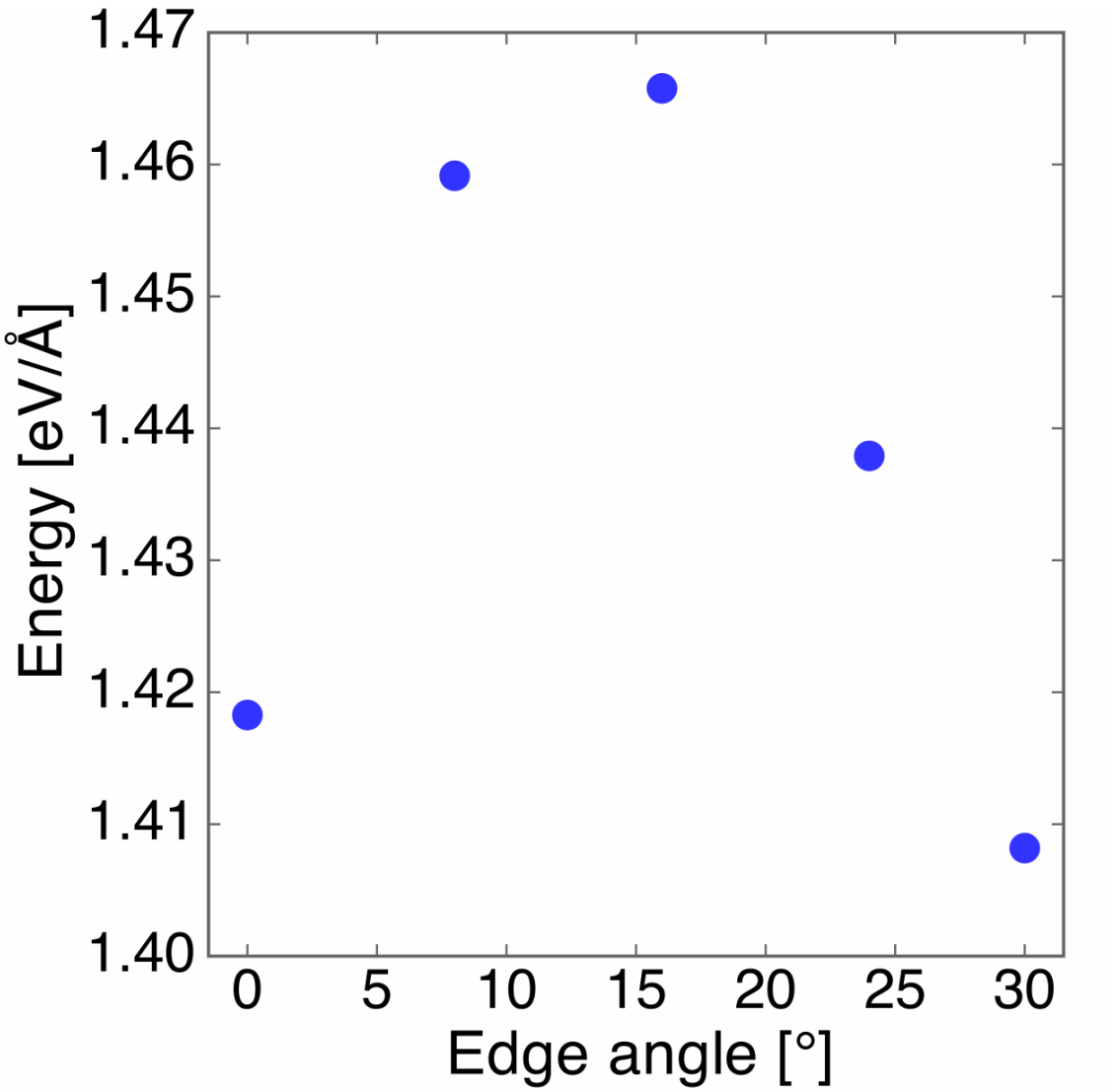

Fig. 2. The edge formation energy per length of MoS_2 nanoribbons with clean edges as a function of the edge angles θ.

their edges [Fig. 1(e)]. However, by carefully checking the bond length of the ribbons with zigzag edges, the edge atomic sites shit inward for both Mo and S, resulting in the decrease the Mo-S bonds along the zigzag edges. These bond length modulation imply that the edge shape of MoS_2 nanoribbon affects their stability and the electronic structures.

To investigate the energetics of the MoS_2 nanoribbons with respect to their edge shape, we calculate the edge formation energy per length of the nanoribbons. The energy

is evaluated by the following equation

$$E = \frac{E_{\text{ribbon}} - N_{\text{MoS}_2}\mu_{\text{MoS}_2}}{L}$$

where E_{ribbon}, N_{MoS_2}, μ_{MoS_2}, and L denote an total energy of the MoS_2 nanoribbons, the number of Mo atoms (48 for all ribbons), a chemical potential of MoS_2 evaluated by an isolated single layer of MoS_2, and the cell parameter along the ribbon direction, respectively. Figure 2 shows the edge formation energy per length of the MoS_2 nanoribbons as a function of the edge angle. The nanoribbon with zigzag edges has the smallest edge formation energy amongst the ribbons studied here. In contrast, the ribbon with chiral edges of which angle is 16° is the least stable. With decrease and increase the edge angle from 16°, the edge formation energy monotonically decreases. Thus, the ribbon with armchair edge is also energetically stable of which energy is higher by 10 meV/Å than that of the ribbon with zigzag edges. Therefore, the MoS_2 nanoflakes prefer zigzag or armchair edges rather than chiral edges. The large energy cost to form chiral edge is ascribed to the boundary between the armchair and zigzag edges, where the edge reconstruction is insufficient to reduce the strain and electron energy.

Figure 3 shows the electronic energy bands and density of states (DOS) of MoS_2 nanoribbons with various edge shapes. The ribbons with edge angles of 0 and 8° are semiconductors with a direct energy gap at the Γ point. The calculated band gaps are 0.54 and 0.17 eV for the ribbons with the edges of the angles of 0 and 8°, respectively. On the other hand, the ribbons with edge angles of 16, 23, and 30° are metals of which electronic structures near the Fermi level are sensitive to the edge shape: dispersive bands cross the Fermi level for the ribbons with edge angles of 16° and 30° (zigzag edge), while the ribbon with the edge angle of 23° has nearly degenerated flat bands at the Fermi level. According to the less dispersive bands around the Fermi level, the ribbon with the edge angle of 23° has relatively large DOS at the Fermi level.

To give the further qualitative insight into the electron states near the Fermi level, we investigate the wave function of the highest branch of the valence band and the lowest branch of the conduction band at the Γ point of the MoS_2 nanoribbons with the clean armchair ($\theta = 0°$), chiral ($\theta = 16°$) and zigzag ($\theta = 30°$) edges (Fig. 4). The wave functions of these states for all nanoribbons are primarily distributed at the edge atomic sites with the unsaturated or dangling bond nature. As for the metallic nanoribbons, electron states associated with the wave function cross the Fermi level so that one-dimensional conducting channels are formed around the edge atomic sites. For

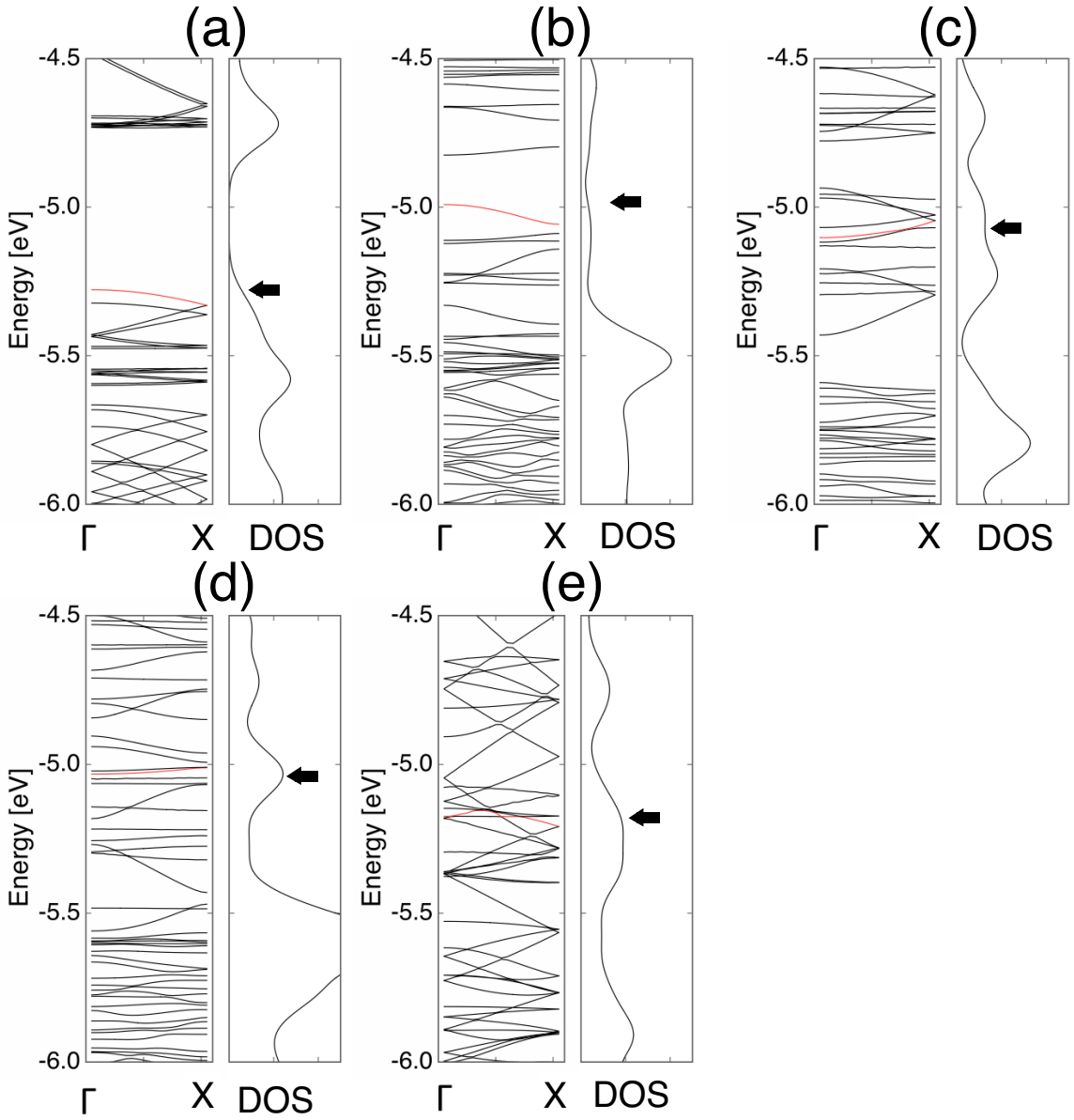

Fig. 3. The electronic energy band and density of states of MoS_2 nanoribbons with clean edges of which angles are (a) 0°, (b) 8°, (c) 16°, (d) 23°, and (e) 30°. Red curves indicate the highest branch of the occupied states. The arrows indicate the valence band edge and the Fermi level energy for the semiconducting and metallic nanorribbons, respectively. Energies are measured from that of the vacuum level.

the case of semiconducting armchair ribbon, electron and hole injection into the conduction and valence bands, respectively, also cause one-dimensional carrier channel at the edge atomic sites: d stats of Mo atoms contribute to the hole transport, while both p and d states of S and Mo atoms, respectively, contribute to the electron transport. Therefore, the conducting channel of MoS_2 nanoribbons with clean edges are robust

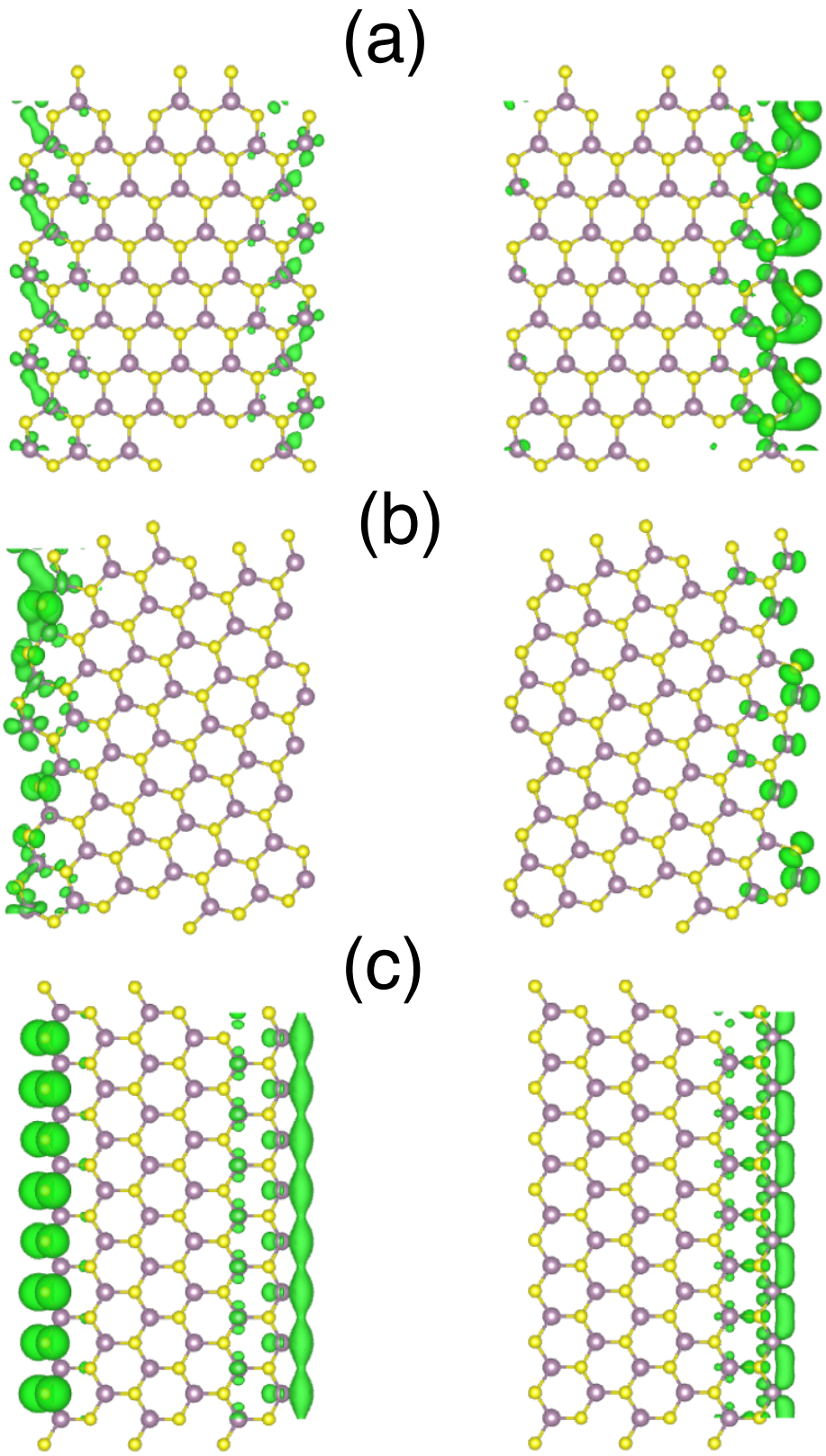

Fig. 4. Isosurfaces of squared wave function of the highest branch of the valence band and the lowest branch of the conduction band of MoS_2 nanoribbons with (a) clean armchair ($\theta = 0°$), (b) clean chiral ($\theta = 16°$), and (c) clean zigzag ($\theta = 30°$) edges. Purple and yellow balls indicate Mo and S atoms, respectively. In each figure, left and right panels correspond with the isosurfaces of HO and LU states, respectively.

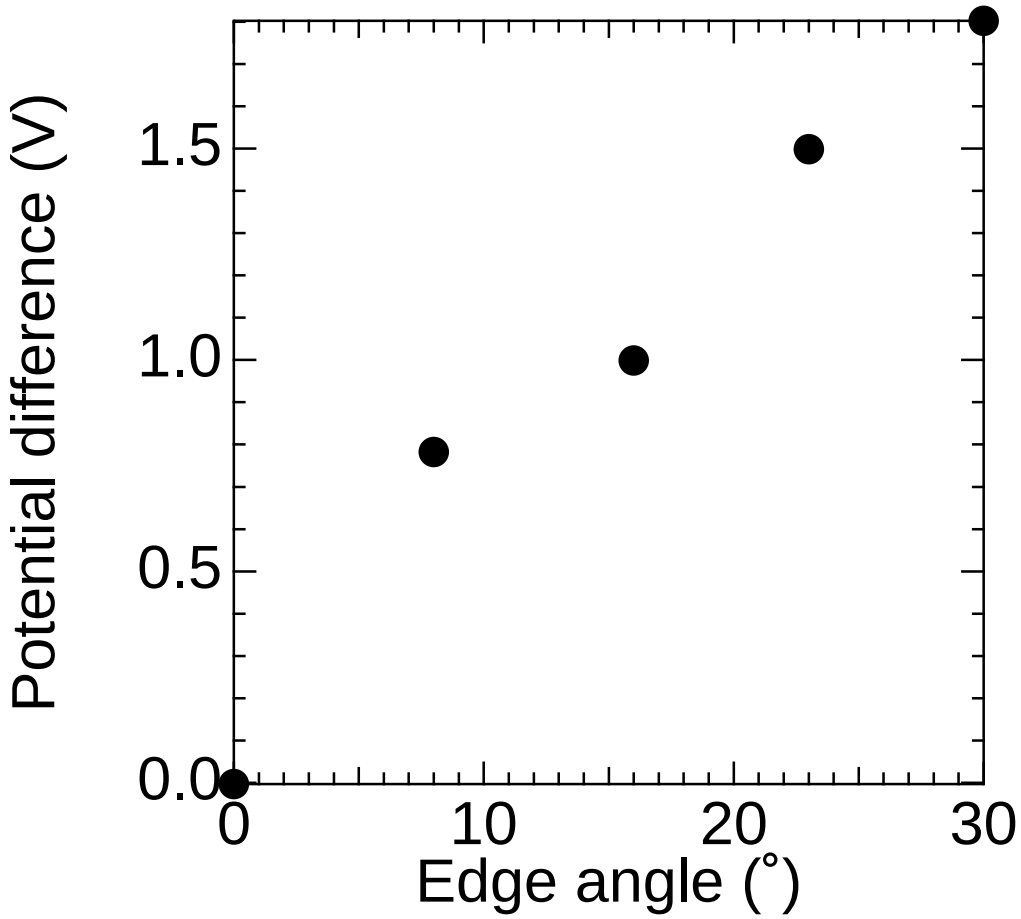

Fig. 5. The electrostatic potential difference between the left and right vacuums of the MoS_2 nanoribbons as a function of edge angle θ. The potential difference is evaluated from the potential at the left vacuum where correspond with S rich edges.

against chemisorption and phyisorption of atoms and molecules on their inner region. However, in contrast, the transport is fragile against the edge termination by functional groups, leading to the further variation in the electronic structures as the edge functionalized graphene nanoribbons.[45] In the case, edge terminations may suppress the dangling bond states at the edge atomic sites, leading to the deterioration of the electron transfer in the metallic nanoribbons.

Since the MoS_2 nanoribbons has asymmetric atomic arrangements in their edges except the ribbons with armchair edges, the nanoribbons with chiral and zigzag edges intrinsically possess the electrostatic polarity across the ribbons. Indeed, by calculating the electrostatic potential across the ribbon, for the most of edge angles, we found a

potential difference between the left (S rich edge) and right (Mo rich edge) vacuum regions of the nanoribbons, except for the ribbon with armchair edges. The potential at the S rich edge is deeper than that at the Mo rich edge because of the intrinsic potential profile of these atoms. Therefore, these results indicated that these MoS_2 nanoribbons have polarity between S and Mo rich edges. Figure 5 shows the edge angle dependence of polarity which is defined as the potential difference between the left and right vacuum regions of the nanoribbons. Because of the symmetric atomic arrangement across the ribbon, the polarity is absent in the ribbons with armchair edges. The polarity is approximately proportional to the edge angle which corresponds with the imbalance between the numbers of Mo and S atoms at the edge atomic sites. Therefore, the polarity of the ribbons are ascribed to their local atomic geometries around the edges. The polarity increased upon increasing the edge with zigzag portion, because of the increase of the imbalance in the number of Mo and S atoms between the two edges. Thus, the fact imply that the MoS_2 nanoribbon is the potential material for piezoelectric devices, because the polarity of the ribbon should strongly depend on the edge atomic structure being sensitive to the external strains.

4. Summary

Using the DFT with ESM method, we conducted comprehensive studies on the energetics and electronic properties of MoS_2 nanoribbons with clean edges in terms of their edge shapes. Our total energy calculation demonstrated that substantial structural reconstruction occurs at the edge atomic site of the nanoribbons: Mo and S shift inward and outward, respectively, under the reconstruction. Accordingly, the edge Mo-S bonds possess a bucked structure for the ribbons except that with zigzag edges. Ribbons with zigzag and armchair edges are relatively stable compared with those with chiral edges. Between the ribbons with armchair and zigzag edges, the formation energy of the zigzag edge is lower by 10 meV than that of the armchair edges, implying the fact that MoS_2 prefers the zigzag edges when the edge is not terminated by atoms or molecules. The electronic structures of the nanoribbons depend on their edge shape: The ribbons with the edge angles of 0° (armchair) and 8° are semiconductors with the direct band gap of 0.54 and 0.17 eV, respectively, at the Γ point. In contrast, the nanoribbons with the edge angles of 16°, 23°, and 30° (zigzag) are metals. Distribution of wave functions associated with the electron state near the Fermi level or the band edges indicate that the most of states are localized at the edge atomic sites, providing one-dimensional channel

for electron and hole conductions. We also found that the electrostatic potential difference between the left and right edges of TMDC nanoribbons, owing to the asymmetric atomic arrangement between the edges, leading to the polar properties of the ribbons. The polarity increased with increasing the zigzag portion at their edges.

Acknowledgements

This work was supported by JST-CREST Grant Numbers JPMJCR1532 and JPMJCR1715 from the Japan Science and Technology Agency, JSPS KAKENHI Grant Numbers JP17H01069, JP16H00898, and JP16H06331 from the Japan Society for the Promotion of Science, and the Joint Research Program on Zero-Emission Energy Research, Institute of Advanced Energy, Kyoto University. Part of the calculations was performed on an NEC SX-Ace at the Cybermedia Center at Osaka University and on an SGI ICE XA/UV at the Institute of Solid State Physics, The University of Tokyo.

References

1) K. S. Novoselov, A. K. Geim, S. V. Morozov, D. Jiang, Y. Zhang, S. V. Dubonos, I. V. Grigorieva, and A. A. Firsov, Science **306**, 666 (2004).
2) M. S. Dresselhaus and G. Dresselhaus, Adv. Phys. **30** 139 (1981).
3) A. H. Castro Neto, F. Guinea, N. M. R. Peres, K. S. Novoselov, and A. K. Geim, Rev. Mod. Phys. **81**, 109 (2009).
4) G. S. Painter and D. E. Ellis, Phys. Rev. B **1**, 4747 (1970).
5) F. Bassani and G.P. Parravicini, Nuovo Cimento B **50**, 95 (1967).
6) M. Posternak, A. Baldereschi, A. J. Freeman, E. Wimmer and M. Weinert, Phys. Rev. Lett. **50**, 761 (1983).
7) Th. Seyller, K. V. Emtsev, K. Gao, F. Speck, L. Ley, A. Tadich, L. Broekman, J. D. Riley, R. C. G. Leckey, O. Rader, A. Varykhalov, and A. M. Shikin, Surf. Sci. **600**, 3906 (2006).
8) J. B. Oostinga, H. B. Heersche, X. Liu, A. F. Morpurgo, and L. M. K. Vandersypen, Nat. Mater. **7**, 151 (2007).
9) Y. Zhang, T. Tang, C. Girit, Z. Hao, M. C. Martin, A. Zettl, M. F. Crommie, Y. R. Shen, and F. Wang, Nature **459**, 820 (2009).
10) I. Forbeaux, J. -M. Themlin, and J. -M. Debever, Phys. Rev. B **58**, 16396 (1998).
11) C. Berger, Z. Song, X. Li, X. Wu, N. Brown, C. Naud, D. Mayou, T. Li, J. Hass, A. N. Marchenkov, E. H. Conrad, P. N. First, and W.A. de Heer, Science **312**, 1191 (2006).
12) H. Ago, Y. Ogawa, M. Tsuji, S. Mizuno, and H. Hibino, J. Phys. Chem. Lett. **3**, 2228 (2012).
13) H. Ago, K. Kawahara, Y. Ogawa, S. Tanoue, M. A. Bissett, M. Tsuji, H. Sakaguchi, R. J. Koch, F. Fromm, T. Seyller, K. Komatsu, and K. Tsukagoshi, Appl. Phys. Express **6**, 075101 (2013).
14) L. Song, L. Ci, H. Lu, P. B. Sorokin, C. Jin, J. Ni, A. G. Kvashnin, D. G. Kvashnin, J. Lou, B. I. Yakobson, and P. M. Ajayan, Nano Lett. **10**, 3209 (2010).
15) Y. Shi, C. Hamsen, X. Jia, K. K. Kim, A. Reina, M. Hofmann, A. L. Hsu, K. Zhang, H. Li, Z. Y. Juang, M. S. Dresselhaus, L. J. Li, and J. Kong, Nano Lett. **10**, 4134 (2010).
16) K. K. Kim, A. Hsu, X. Jia, S. M. Kim, Y. Shi, M. Hofmann, D. Nezich, J. F. Rodriguez-Nieva, M. Dresselhaus, T. Palacios, and J. Kong, Nano Lett. **12**, 161

(2012).

17) S. Helveg, J. V. Lauritsen, E. Lægsgaard, I. Stensgaard, J.K. Nørskov, B.S. Clausen, H. Topsøe and F. Besenbacher, Phys. Rev. Lett. **84**, 951 (2000).
18) K. F. Mak, Ch. Lee, J. Hone, J. Shan, and T. F. Heinz, Phys. Rev. Lett. **105**, 136805 (2010).
19) N. T. Cuong, M. Otani, and S. Okada, J. Phys.: Condens. Matter **26**, 135001 (2014).
20) A. K. Geim and I. V. Grigorieva, nature **499**, 419 (2013).
21) S. Masubuchi, M. Morimoto, S. Morikawa, M. Onodera, Y. Asakawa, K. Watanabe, T. Taniguchi, and T. Machida, Ntr. Commun. **9**, 1413 (2018).
22) S. Iijima, Nature **354**, 56 (1991).
23) N. Hamada, S. Sawada, and A. Oshiyama, Phys. Rev. Lett. **68**, 1579 (1992).
24) R. Saito, M. Fujita, M. S. Dresselhaus, and G. Dresselhaus, Appl. Phys. Lett. **60**, 2204 (1992).
25) M. Fujita, K. Wakabayashi, K. Nakada, and K. Kusakabe, J. Phys. Soc. Jpn. **65**, 1920 (1996).
26) K. Nakada, M. Fujita, G. Dresselhaus, and M. S. Dresselhaus, Phys. Rev. B **54**, 17954 (1996).
27) S. Okada and A. Oshiyama, Phys. Rev. Lett. **87**, 146803 (2001).
28) A. Yamanaka and S. Okada, Carbon **96**, 351(2016).
29) S. Okada, Phys. Rev. B **77**, 041408 (2008).
30) S. Okada, M. Igami, K. Nakada, and A. Oshiyama, Phys. Rev. B **62**, 9896 (2000).
31) A. Yamanaka and S. Okada, Sci. Rep. **6**, 30653 (2016).
32) M. Maruyama and S. Okada, Sci. Rep. **8**, 16657 (2018).
33) R. Tenne, L. Margulis, M. Genut, and G. Hodes, Nature **360**, 444 (1992).
34) J. Lin, O. Cretu, W. Zhou, K. Suenaga, D. Prasai, K. I. Bolotin, N. T. Cuong, M. Otani, S. Okada, A. R. Lupini, J.-C. Idrobo, D. Caudel, A. Burger, N. J. Ghimire, J. Yan, D. G. Mandrus, S. J. Pennycook, and S. T. Pantelides, Ntr. Nanotechnol. **9**, 436 (2014).
35) M. V. Bollinger, J. V. Lauritsen, K. W. Jacobsen, J. K. Nørskov, S. Helveg, and F. Besenbacher, Phys. Rev. Lett. **87**, 196803 (2001).
36) Q. Yue, S. Chang, J. Kang, X. Zhang, Z. Shao, S. Qin, and J. Li, J. Phys.: Condens. Matter **24**, 335501 (2012).
37) Y. Li, Z. Zhou, S. Zhang, and Z. Chen, J. Am. Chem. Soc. **130**, 16739 (2008).

38) P. Hohenberg and W. Kohn, Phys. Rev. **136**, B864 (1964).
39) W. Kohn and L. J. Sham, Phys. Rev. **140**, A1144 (1965).
40) Y. Morikawa, K. Iwata, and K. Terakura, Appl. Surf. Sci. **169-170**, 11 (2001).
41) J. P. Perdew, K. Burke, and M. Ernzerhof, Phys. Rev. Lett. **77**, 3865 (1997).
42) J. P. Perdew, K. Burke, and M. Ernzerhof, Phys. Rev. Lett. **78**, 1396 (1997).
43) D. Vanderbilt, Phys. Rev. B **41**, 7892 (1990).
44) M. Otani and O. Sugino, Phys. Rev. B **73**, 115407 (2006).
45) R. Taitra, A. Yamanaka, and S. Okada, Appl. Phys. Express **9**, 115102 (2016).